Canonical scale separation in two-dimensional incompressible hydrodynamics

J. Fluid Mech. (2022), *vol*. 943, A36, doi:10.1017/jfm.2022.457

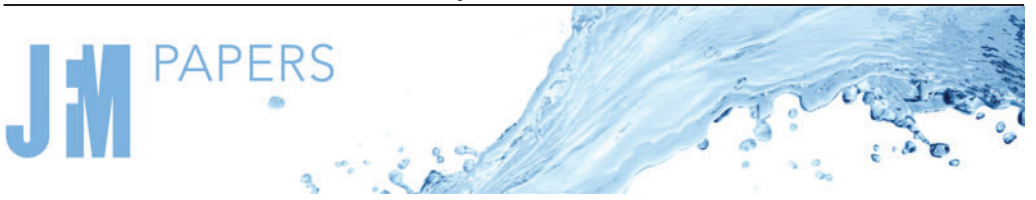

Canonical scale separation in two-dimensional incompressible hydrodynamics

Klas Modin[1],† **and Milo Viviani**[2]

[1]Chalmers University of Technology and University of Gothenburg, Gothenburg, Sweden

[2]Scuola Normale Superiore di Pisa, Pisa, Italy

(Received 31 May 2021; revised 3 May 2022; accepted 16 May 2022)

The rules that govern a two-dimensional inviscid incompressible fluid are simple. Yet, to characterise the long-time behaviour is a knotty problem. The fluid fulfils Euler's equations: a nonlinear Hamiltonian system with an infinite number of conservation laws. In both experiments and numerical simulations, coherent vortex structures emerge after an initial stage. These formations dominate the large-scale dynamics, but small scales also emerge and persist. The resulting scale separation resembles Kraichnan's theory of forward and backward cascades of enstrophy and energy. Previous attempts to model the double cascade use filtering techniques that enforce separation from the outset. Here, we show that Euler's equations possess an intrinsic, canonical splitting of the vorticity function. The splitting is remarkable in four ways: (i) it is defined solely by the Poisson bracket and the Hamiltonian; (ii) it characterises steady flows; (iii) it innately separates scales, enabling the dynamics behind Kraichnan's qualitative description; and (iv) it accounts for 'broken line' energy spectra observed in both experiments and numerical simulations. The splitting originates from Zeitlin's truncated model of Euler's equations in combination with a standard quantum tool: the spectral decomposition of Hermitian matrices. In addition to theoretical insight, the scale separation dynamics enables stochastic model reduction, where multiplicative noise models small scales.

Key words: Hamiltonian theory, computational methods

1. Introduction

Two-dimensional turbulence is the study of incompressible hydrodynamics at large (including infinite) Reynolds numbers. It is a vibrant field of both mathematics and physics that began with Euler (1757), who derived the basic equations of motion. Turbulent flows in

† Email address for correspondence: klas.modin@chalmers.se

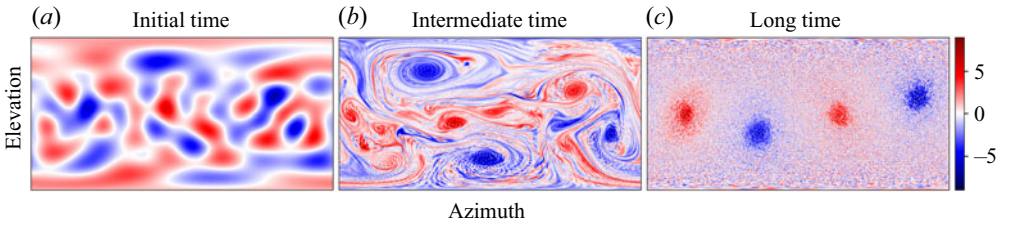

Figure 1. Evolution of vorticity for Euler's equations on the sphere. Vorticity regions of equal sign undergo merging to form stable, interacting vortex condensates.

two space dimensions do not exist as classical fluids in nature. Rather, they constitute basic models of intermediate-scale flows in 'almost' two-dimensional (thin) domains (Majda & Bertozzi 2002; Cullen 2006; Majda & Wang 2006; Dolzhansky 2013; Pedlosky 2013; Zeitlin 2018).

The conditions of two-dimensional (2-D) turbulence can be emulated in experiments. One set-up is a soap film flowing rapidly through a fine comb (Couder 1984). Another is a conducting fluid confined to a thin layer and driven into turbulence by a temporally varying magnetic field (Sommeria 1988). When such a 'quasi-2-D' flow is released it self-organises into blob-like condensates. The progression is depicted in figure 1 for a spherical domain. Heuristically, the mechanism is driven by the merging of equally signed vorticity regions. This large-scale fusion is balanced by fine-scale dissipation. In many ways, 2-D turbulence is propelled by the quest to understand the resulting scale separation.

To make theoretical progress, Onsager (1949) applied statistical mechanics to a large but finite number N of point vortices. They are weak (distributional) solutions of Euler's equations where vorticity is a sum of weighted Dirac pulses. Onsager realised that a fixed number of positive and negative point vortices, confined to a bounded domain, can have energies from $-\infty$ to ∞. The phase volume function, therefore, has an inflexion point at some finite energy. At this energy, the thermodynamical temperature is zero. If the energy exceeds this point, so the temperature is negative, then equally signed vortices should cluster according to thermodynamics. This theory of statistical hydrodynamics is a prominent, although lesser-known, part of Onsager's legacy (Eyink & Sreenivasan 2006). Its validation is a long-standing open problem (Marchioro & Pulvirenti 2012, discussion in chap. 7). On the mathematical side, Caglioti *et al.* (1992, 1995) and Kiessling (1993) gave rigorous results on clustering of point vortices in the negative temperature regime as $N \to \infty$ under the assumption of ergodicity. Their work has fostered much theoretical progress (Marchioro & Pulvirenti 2012, and references therein). On the experimental side, seventy years after Onsager presented his theory, the conditions of negative temperature point vortex dynamics were experimentally realised in planar Bose–Einstein condensates (Gauthier *et al.* 2019; Johnstone *et al.* 2019). As predicted, persisting vortex clusters emerge.

Onsager's theory cannot be applied to continuous vorticity fields (corresponding to smooth solutions). Consequently, it is natural to look for a statistical theory of continua. One approach is to expand the vorticity field in a Fourier series and then truncate it (Kraichnan 1975). The truncated, finite-dimensional system preserves phase volume and quadratic invariants, but not higher-order invariants (Casimir functions). To account also for those invariants, another approach is to maximise the entropy of a probability distribution of coarse-grained vorticity fields (Lynden-Bell 1967; Miller 1990; Robert & Sommeria 1991).

All theories based on statistical mechanics assume an ergodic dynamics. Rigorous results on ergodicity are available for 2-D Navier–Stokes on a doubly periodic domain (flat torus) with added regular-in-space noise proportional to the square root of the viscosity ν. In this setting there exists a unique stationary measure μ_ν (Kuksin & Shirikyan 2012, 2017). As $\nu \to 0$, one obtains a stationary measure μ_0 for the 2-D Euler equations, but it is not expected to be unique (Kuksin & Shirikyan 2017).

Statistical mechanics is not the only approach. Another possibility is to study energy and enstrophy spectra. The inspiration comes from Kolmogorov's (1941) theory of 3-D turbulence. Notably, Kraichnan (1967) argued that viscous 2-D fluids in forced equilibrium, where energy at an intermediate scale is fed into the system, exhibit a forward cascade of enstrophy into fine scales and a simultaneous backward cascade of energy into large scales. Direct numerical simulations typically support Kraichnan's theory (Xiao *et al.* 2009, and references therein).

For 2-D systems with no energy dissipation at the large scale (so that vortex condensation occurs), numerical simulations develop a 'broken line' energy spectrum with a steep slope at the large scale, typically steeper than k^{-3} where k is the wavenumber, and then a swift switch at an intermediate scale to a less steep slope, typically between $k^{-5/3}$ and k^{-1} (Boffetta & Ecke 2012, and references therein). An approximate broken line energy spectrum is also observed in zonal and meridional wind measurements on Earth over the scales 3–10 000 km (Nastrom, Gage & Jasperson 1984).

To better understand characteristic energy spectra it is natural to impose a splitting of the vorticity field $\omega = \omega_s + \omega_r$ into a large-scale component ω_s and a small-scale component ω_r. A wavelet-based vorticity splitting is proposed by Farge, Schneider & Kevlahan (1999) and applied to numerical simulation on the doubly periodic square (where condensation occurs) by Chertkov *et al.* (2007). The results (Chertkov *et al.* 2007, figure 1*f*) show an energy spectrum slope of k^{-3} for the large-scale component and of k^{-1} for the intermediate-to-small-scale component. It is a powerful technique to analyse energy spectra, but it depends on a choice of wavelet basis and parameters identifying the different scales. Therefore, the method cannot give insights into the mechanisms behind vortex condensation or broken line energy spectra.

In this paper, we give a new, canonical decomposition of vorticity. By 'canonical' we mean parameter free, determined solely in terms of the data for the 2-D Euler equations: the Poisson bracket and the Hamiltonian function. The decomposition has the following properties:

(i) The vorticity field $\omega = \omega_s + \omega_r$ is a steady state if and only if $\omega_r = 0$.
(ii) Under numerical simulation of Euler's equations, ω_s and ω_r evolve into a separation of scales. The component ω_s traps large-scale condensates whereas the component ω_r captures small-scale fluctuations.
(iii) After a short transient time, the energy spectrum slope of ω_s is approximately k^{-3} and that of ω_r is between $k^{-5/3}$ and k^{-1}.
(iv) Over time, the component ω_r displays an average enstrophy increase (quantifying the forward enstrophy cascade) and an average energy decrease (quantifying the backward energy cascade).

The coupled equations governing the dynamics of ω_s and ω_r embody a new line of attack for 2-D turbulence. Our standpoint is that a detailed study of these equations may explain the mechanisms behind vortex condensation and broken line energy spectra, or at least give deep insights. The numerical simulations we present suggest so.

1.1. *Two-dimensional Euler equations*

Our starting point is Euler's equations for an inviscid, incompressible fluid on a 2-D closed surface. Throughout the paper, we take the surface to be the unit sphere $\mathbb{S}^2 \subset \mathbb{R}^3$. It makes our arguments more explicit and enables numerics. Most concepts are readily transferable to arbitrary closed surfaces (in particular to the flat torus, which is the most studied example in the literature albeit less relevant than the sphere in applications).

In vorticity formulation, Euler's equations on $\mathbb{S}^2$ are

$$\dot{\omega} = \{\psi, \omega\}, \quad \Delta\psi = \omega, \tag{1.1a,b}$$

where $\{\cdot,\cdot\}$ is the Poisson bracket on $\mathbb{S}^2$, ω is the vorticity function of the fluid, related to the fluid velocity $\boldsymbol{v}$ via $\omega = \operatorname{curl}\boldsymbol{v}$, and ψ is the streamfunction, related to the vorticity function via the Laplace–Beltrami operator Δ. Geometrically, (1.1*a*,*b*) constitute an infinite-dimensional Lie–Poisson system (Arnold & Khesin 1998, and references therein). The phase space consists of vorticity fields and is equipped with the following infinite-dimensional Poisson bracket:

$$\prec F, G \succ (\omega) = \int_{\mathbb{S}^2} \left\{ \frac{\delta F}{\delta \omega}, \frac{\delta G}{\delta \omega} \right\} \omega. \tag{1.2}$$

The Hamiltonian (total energy) for the vorticity equation (1.1*a*,*b*) is

$$H = -\tfrac{1}{2} \int_{\mathbb{S}^2} \psi\omega. \tag{1.3}$$

In addition to total energy, there is an infinite number of conservation laws: total angular momentum

$$\boldsymbol{L} = \int_{\mathbb{S}^2} \omega \boldsymbol{n}, \quad \boldsymbol{n} \text{ unit normal on } \mathbb{S}^2, \tag{1.4}$$

and Casimir functions

$$C_f(\omega) = \int_{\mathbb{S}^2} f(\omega), \quad \text{for any smooth } f\colon \mathbb{R} \to \mathbb{R}. \tag{1.5}$$

These conservation laws are fundamental for long-time behaviour. In particular, the presence of infinitely many Casimir functions sets apart 2-D from 3-D fluids.

1.2. *Overview of the paper*

Zeitlin's truncated model of Euler's equations originates from the vorticity formulation (1.1*a*,*b*). In the spirit of quantisation theory, the space of vorticity functions is replaced by the space $\mathfrak{u}(N)$ of skew-Hermitian complex matrices, while the Poisson bracket is replaced by the matrix commutator. The size N of the matrices is the spatial discretisation parameter, related to 'Planck's constant' in quantum theory via $\hbar = 1/N$. We present an overview of how functions and matrices are related in § 2.

There are at least two advantages of Zeitlin's model. First, it yields a spatial discretisation that preserves all the underlying geometry of the Euler equations: the Hamiltonian structure and the conservation laws. Combined with a symplectic time-integration scheme one can obtain fully structure-preserving numerical methods (Modin & Viviani 2020*a*). Second, complicated topological or geometrical properties of the Euler equations can be described in terms of standard tools from linear algebra and matrix Lie groups. Indeed, our splitting naturally arises from the standard spectral decomposition of Hermitian matrices applied to the stream matrix. The splitting has a

precise geometric meaning in terms of Lie algebras, but also a dynamical interpretation as the steady and unsteady vorticity components. The details are given in § 3.

Numerical experiments for the canonical splitting are presented and discussed in § 4. We demonstrate that the components in the splitting converge into a separation of scales. They also capture broken line energy spectra. To rigorously answer to what degree simulations based on Zeitlin's model capture the behaviour of Euler's equations is an open problem.

In § 5 we translate our results about Zeitlin's model to the continuous Euler equations. All matrix concepts used for the canonical splitting have classical, fluid dynamical counterparts. But to define them rigorously requires prudence. It is essential to use a weak formulation. The section sets the foundation for an L^∞-based theory of canonical vorticity splitting, independent of Zeitlin's model. It is the most mathematical part of the paper. Even so, a heuristic explanation is straightforward. Let us give it here. For a smooth vorticity function ω, the aim is to construct a splitting $\omega = \omega_s + \omega_r$. Let $\boldsymbol{\gamma}(\tau)$ be a closed level curve of ψ. We define ω_s, restricted to $\boldsymbol{\gamma}$, to take the constant value

$$\omega_s|_{\boldsymbol{\gamma}} = \frac{1}{\text{length}(\boldsymbol{\gamma})} \int_{\boldsymbol{\gamma}} \omega \, \mathrm{d}\tau. \tag{1.6}$$

In other words, ω_s is obtained via averaging of ω along the level curves, or streamlines, of ψ. The mathematical difficulties arise where the level curves contain bifurcations.

2. Background to Euler–Zeitlin equations

In this section we give background to the 'consistent truncation' of Euler's equations introduced by Zeitlin (1991, 2004). The model relies on quantisation of the Poisson algebra of smooth functions (Hoppe 1982; Fairlie & Zachos 1989). Recall that the Poisson bracket between two smooth functions $f, g \in C^\infty(\mathbb{S}^2)$ is

$$\{f, g\}(\boldsymbol{x}) = \boldsymbol{x} \cdot (\nabla f \times \nabla g), \quad \boldsymbol{x} \in \mathbb{S}^2 \subset \mathbb{R}^3. \tag{2.1}$$

Quantisation, in our context, means to find a projection from smooth functions $C^\infty(\mathbb{S}^2)$ to complex skew-Hermitian matrices $\mathfrak{u}(N)$ such that the Poisson bracket (2.1) under this map is approximated by the matrix commutator.

On the sphere, quantisation is explicit, obtained as follows. Hoppe & Yau (1998) gave an operator $\Delta_N \colon \mathfrak{u}(N) \to \mathfrak{u}(N)$ with the same spectrum as the Laplace–Beltrami operator (up to truncation N). The eigenvectors $\boldsymbol{T}^N_{lm}$ of Δ_N are the quantised analogues of the spherical harmonics Y_{lm}. It is therefore natural to define the projection $\Pi_N \colon C^\infty(\mathbb{S}^2) \to \mathfrak{u}(N)$ mapping functions to matrices via

$$C^\infty(\mathbb{S}^2) \ni \omega = \sum_{l=0}^{\infty} \sum_{m=-l}^{l} \omega^{lm} Y_{lm} \mapsto \sum_{l=0}^{N} \sum_{m=-l}^{l} \omega^{lm} \boldsymbol{T}^N_{lm} = W \in \mathfrak{u}(N). \tag{2.2}$$

For more details and explicit formulae we refer to Hoppe & Yau (1998), Zeitlin (2004) and Modin & Viviani (2020*a*).

The vorticity formulation (1.1*a*,*b*) uses only the Laplacian Δ and the Poisson bracket $\{\cdot, \cdot\}$. Their quantised analogues Δ_N and $[\cdot, \cdot]$ give rise to the Euler–Zeitlin equations

$$\dot{\boldsymbol{W}} = [\boldsymbol{P}, \boldsymbol{W}], \quad \Delta_N \boldsymbol{P} = \boldsymbol{W}, \tag{2.3a,b}$$

where $\boldsymbol{W} \in \mathfrak{su}(N)$ is the vorticity matrix and $\boldsymbol{P} \in \mathfrak{su}(N)$ is the stream matrix. The condition

$$\boldsymbol{W} \in \mathfrak{su}(N) = \{\boldsymbol{A} \in \mathfrak{u}(N) \mid \operatorname{tr} \boldsymbol{A} = 0\} \tag{2.4}$$

corresponds to vanishing total circulation $\int_{\mathbb{S}^2} \omega = 0$.

The Euler–Zeitlin equations (2.3*a*,*b*) have been studied in various contexts, primarily on the flat torus (Zeitlin 1991; McLachlan 1993; Abramov & Majda 2003), but also on the sphere (Zeitlin 2004; Modin & Viviani 2020*a*). Their main feature is that they preserve the rich phase space geometry of the original equations (1.1*a*,*b*), namely the Lie–Poisson structure (Modin & Viviani 2020*a*,*c*, and references therein). In turn, this structure implies conservation of total energy $H(\boldsymbol{W}) = \mathrm{Tr}(\boldsymbol{PW})/2$, (quantised) Casimirs $C_k(\boldsymbol{W}) = \mathrm{Tr}(\boldsymbol{W}^k)$ and angular momentum $\boldsymbol{L} = (L_x, L_y, L_z)$. Conventional discretisations do not maintain these conservation laws.

REMARK 2.1. *Quantisation on the sphere is more complicated to work with than quantisation on the torus. Even so, the Euler–Zeitlin equations are more accurate on the sphere than on the torus. This has a deep geometric reason: quantisation exactly preserves the rotational symmetry of the sphere, but the translational symmetry of the torus is only approximately captured. The quantised Poisson equation on the torus, therefore, suffers from the Gibbs phenomenon, which is not present on the sphere.*

In previous work (Modin & Viviani 2020*a*,*c*) we develop a Lie–Poisson-preserving numerical method for the Euler–Zeitlin equations on the sphere and we use it to study the long-time behaviour. Our numerical results, along with earlier ones by Dritschel, Qi & Marston (2015), give strong evidence against the predictions of statistical mechanics theories, derived for the sphere by Herbert (2013); see also Bouchet & Venaille (2012). Rather, the results suggest the existence of near-integrable parts of phase space that act as barriers for the statistical predictions to be reached. Those near-integrable solutions take the form of interacting vortex blobs (3 or 4 depending on the total angular momentum), perfectly reflecting integrability conditions for the Hamiltonian dynamics on the sphere (Modin & Viviani 2021).

During our work with Zeitlin's model, a new point of view emerged. More than a spatial discretisation, the Euler–Zeitlin equations themselves provide new mathematical tools 2-D hydrodynamics. Those tools include, in particular, Lie theory for $\mathfrak{u}(N)$, which is exceptionally well understood from quantum theory, representation theory and linear algebra. In particular, through the lens of Lie algebra theory, it is natural to split the vorticity matrix $\boldsymbol{W}$ by orthogonal projection onto the stabiliser of the stream matrix $\boldsymbol{P}$ – the underpinning point of this paper. By simulating the Euler–Zeitlin equations (2.3*a*,*b*) using our Lie–Poisson integrator, and then for each output computing the canonical splitting, we see that it captures the dynamics of vortex condensation and scale separation, directly related to the theory of Kraichnan (1967) for an inverse energy cascade.

3. Canonical splitting of the vorticity matrix

In this section, we present and discuss canonical vorticity splitting for Zeitlin's model. Here, 'canonical' means that the splitting only depends on the Lie algebra structure, the vorticity matrix $\boldsymbol{W}$ and the stream matrix P. It does not require any *ad hoc* choice of scale as previous methods do. The scale separation is a result of the dynamics itself.

Consider again the Euler–Zeitlin equations (2.3*a*,*b*). Equip $\mathfrak{su}(N)$ with the Frobenius inner product. The canonical splitting of the vorticity matrix

$$\boldsymbol{W} = \boldsymbol{W}_s + \boldsymbol{W}_r \tag{3.1}$$

is obtained by taking $\boldsymbol{W}_s$ to be the orthogonal projection of $\boldsymbol{W}$ onto the stabiliser of the stream matrix $\boldsymbol{P}$

$$\mathrm{stab}_{\boldsymbol{P}} = \{\boldsymbol{A} \in \mathfrak{su}(N) \mid [\boldsymbol{A}, \boldsymbol{P}] = 0\}. \tag{3.2}$$

If $\boldsymbol{P}$ is generic, then all its eigenvalues are distinct, and $\mathrm{stab}_{\boldsymbol{P}}$ is equivalently given by

$$\mathrm{stab}_{\boldsymbol{P}} = \{\boldsymbol{A} \in \mathfrak{su}(N) \mid \boldsymbol{A}, \boldsymbol{P} \text{ simultaneously diagonalisable}\}. \tag{3.3}$$

In this case $\boldsymbol{W}_s$ is obtained via the spectral decomposition: first find $\boldsymbol{E} \in \mathrm{SU}(N)$ that diagonalises $\boldsymbol{P}$, then define $\Pi_{\boldsymbol{P}}\colon \mathfrak{su}(N) \to \mathrm{stab}_{\boldsymbol{P}}$ as

$$\boldsymbol{W}_s := \Pi_{\boldsymbol{P}}(\boldsymbol{W}) = \boldsymbol{E}\,\mathrm{diag}(\boldsymbol{E}^\dagger \boldsymbol{W}\boldsymbol{E})\boldsymbol{E}^\dagger. \tag{3.4}$$

REMARK 3.1. *Relative to the splitting* (3.1)*, the Euler–Zeitlin equations* (2.3*a*,*b*) *can be written*

$$\dot{\boldsymbol{W}} = [\boldsymbol{P}, \boldsymbol{W}_r]. \tag{3.5}$$

In fact, $\boldsymbol{W} = \boldsymbol{W}_s + \boldsymbol{W}_r$ *is a steady solution (equilibrium) if and only if* $\boldsymbol{W}_r = 0$*. So, in a way, the dynamics emerges from the residual part* $\boldsymbol{W}_r$*.*

3.1. *Dynamics of* $\boldsymbol{W}_s$ *and* $\boldsymbol{W}_r$

For insight into the splitting (3.1) we derive the Euler–Zeitlin equations in the variables $\boldsymbol{W}_s$ and $\boldsymbol{W}_r$. Consider first a general flow on $\mathfrak{su}(N)$ of the form

$$\dot{\boldsymbol{P}} = F(\boldsymbol{P}), \tag{3.6}$$

for some smooth vector field $F\colon \mathfrak{su}(N) \to \mathfrak{su}(N)$. Let $\boldsymbol{E} \in \mathrm{SU}(N)$ and $\boldsymbol{\Lambda} \in \mathrm{diag}_N$ denote an eigenbasis and corresponding eigenvalues for $\boldsymbol{P}$. Given (3.6) we first determine the evolution of $\boldsymbol{E}$ and $\boldsymbol{\Lambda}$. The Lie algebra $\mathfrak{su}(N)$ is foliated in orbits (cf. Kirillov 2004) given by

$$O_{\boldsymbol{P}} = \{\boldsymbol{U}\boldsymbol{P}\boldsymbol{U}^\dagger \mid \boldsymbol{U} \in \mathrm{SU}(N)\}. \tag{3.7}$$

In the generic case, when all eigenvalues are distinct, the tangent space $T_{\boldsymbol{P}}O_{\boldsymbol{P}}$ is spanned by $\{\mathrm{i}e_k e_l^\dagger\}_{k \neq l}$, where $\boldsymbol{E} = [e_1, \ldots, e_N]$ is an orthonormal eigenbasis of $\boldsymbol{P}$. The orthogonal directions $T_{\boldsymbol{P}}O_{\boldsymbol{P}}^\perp = \mathrm{span}\{\mathrm{i}e_k e_k^\dagger\} = \mathrm{stab}_{\boldsymbol{P}}$ are the linear subspace of matrices in $\mathfrak{su}(N)$ sharing the same eigenbasis (they are simultaneously diagonalisable). Thus, the two projections

$$\Pi_{\boldsymbol{P}}\colon \mathfrak{su}(N) \to \mathrm{stab}_{\boldsymbol{P}} \quad \text{and} \quad \Pi_{\boldsymbol{P}}^\perp := \mathrm{Id} - \Pi_{\boldsymbol{P}}\colon \mathfrak{su}(N) \to \mathrm{stab}_{\boldsymbol{P}}^\perp \tag{3.8a,b}$$

correspond to decomposition in the basis $\{\mathrm{i}e_k e_k^\dagger\}_k$ and $\{\mathrm{i}e_k e_l^\dagger\}_{k \neq l}$. Notice, as expected, that neither $\Pi_{\boldsymbol{P}}$ nor $\Pi_{\boldsymbol{P}}^\perp$ depend on the eigenvalues of $\boldsymbol{P}$, only on the eigenbasis.

We can now write (3.6) as

$$\dot{\boldsymbol{P}} = \Pi_{\boldsymbol{P}}F(\boldsymbol{P}) + \Pi_{\boldsymbol{P}}^\perp F(\boldsymbol{P}). \tag{3.9}$$

The first part of the flow changes the eigenbasis but not the eigenvalues and *vice versa*. The question is: What is the generator of $\boldsymbol{P} \mapsto \Pi_{\boldsymbol{P}}^\perp F(\boldsymbol{P})$? Since it is isospectral it should

be of the form $\boldsymbol{P} \mapsto [B(\boldsymbol{P}), \boldsymbol{P}]$ for some $B(\boldsymbol{P}) \in \mathfrak{su}(N)$. Let us denote $X = F(\boldsymbol{P})$. If the eigenvalues $p_1, \dots, p_N$ of $\boldsymbol{P}$ are distinct, then

$$\begin{aligned} \Pi_{\boldsymbol{P}}^{\perp} \boldsymbol{X} &= \sum_{k \neq l} x_{kl} \mathrm{i} e_k e_l^\dagger = \sum_{k \neq l} (p_k - p_l) b_{kl} e_k e_l^\dagger \\ &= \left[\sum_{k \neq l} b_{kl} e_k e_l^\dagger, \boldsymbol{P} \right] = [\boldsymbol{B}, \boldsymbol{P}], \end{aligned} \tag{3.10}$$

where x_{kl} are the components of $\boldsymbol{X}$ in the basis $\boldsymbol{E}$, and $b_{kl} \coloneqq x_{kl}/(p_k - p_l)$. Thus, in the generic case the generator $B(\boldsymbol{P})$ is constructed from the eigenvalues $p_1, \dots, p_N$ and the eigenbasis $e_1, \dots, e_N$ of $\boldsymbol{P}$. This observation allows us to write (3.6) in terms of the eigenvalues and eigenbasis of $\boldsymbol{P}$

$$\left.\begin{aligned} \dot{p}_k &= e_k^\dagger \boldsymbol{X} e_k, \quad \boldsymbol{X} = F\left(\sum_{k=1}^{N} p_k e_k e_k^\dagger \right) \\ \dot{e}_k &= \boldsymbol{B} e_k, \quad \boldsymbol{B} = \sum_{k \neq l} \frac{e_k^\dagger \boldsymbol{X} e_l}{p_k - p_l} e_k e_l^\dagger. \end{aligned}\right\} \tag{3.11}$$

The matrices $\boldsymbol{E}_{kk} = \mathrm{i} e_k e_k^\dagger \in \mathfrak{su}(N)$, forming the eigenbasis of $\boldsymbol{P}$, are the quantised analogues of the level curves of the streamfunction ψ.

We now apply the Lie theory machinery to obtain the dynamics of $\boldsymbol{W}_s$ and $\boldsymbol{W}_r$. From the definition of $\boldsymbol{W}_s$ we have

$$\begin{aligned} \dot{\boldsymbol{W}}_s &= \frac{\mathrm{d}}{\mathrm{d}t} (\boldsymbol{E} \operatorname{diag}(\boldsymbol{E}^\dagger \boldsymbol{W} \boldsymbol{E}) \boldsymbol{E}^\dagger) \\ &= [\dot{\boldsymbol{E}} \boldsymbol{E}^\dagger, \boldsymbol{W}_s] - \Pi_P([\dot{\boldsymbol{E}} \boldsymbol{E}^\dagger, \boldsymbol{W}_r]), \end{aligned} \tag{3.12}$$

where we used $\Pi_P(\dot{\boldsymbol{W}}) = 0$ and $\dot{\boldsymbol{E}} \boldsymbol{E}^\dagger = -\boldsymbol{E} \dot{\boldsymbol{E}}^\dagger$. The dynamics for $\boldsymbol{P}$ is similar

$$\dot{\boldsymbol{P}} = [\dot{\boldsymbol{E}} \boldsymbol{E}^\dagger, \boldsymbol{P}] + \boldsymbol{E} \dot{\boldsymbol{\Lambda}} \boldsymbol{E}^\dagger. \tag{3.13}$$

Hence, a formula for $\dot{\boldsymbol{E}} \boldsymbol{E}^\dagger$ is needed. But we know that the dynamics of $\boldsymbol{P}$ can be orthogonally decomposed as

$$\dot{\boldsymbol{P}} = \Pi_{\boldsymbol{P}}^{\perp} (\Delta_N^{-1} [\boldsymbol{P}, \Delta \boldsymbol{P}]) + \Pi_{\boldsymbol{P}} (\Delta_N^{-1} [\boldsymbol{P}, \Delta \boldsymbol{P}]), \tag{3.14}$$

so

$$[\dot{\boldsymbol{E}} \boldsymbol{E}^\dagger, \boldsymbol{P}] = \Pi_{\boldsymbol{P}}^{\perp} (\Delta_N^{-1} [\boldsymbol{P}, \Delta \boldsymbol{P}]). \tag{3.15}$$

Notice that $\dot{\boldsymbol{E}} \boldsymbol{E}^\dagger$ can be taken in $\mathrm{stab}_P^{\perp}$. In fact, the dynamics of $\boldsymbol{W}_s$ remains the same for any $\dot{\boldsymbol{E}} \boldsymbol{E}^\dagger + \boldsymbol{S}$ with $\boldsymbol{S} \in \mathrm{stab}_{\boldsymbol{P}}$. The map

$$[\cdot, \boldsymbol{P}] : \mathrm{stab}_{\boldsymbol{P}}^{\perp} \to \mathrm{stab}_{\boldsymbol{P}}^{\perp} \tag{3.16}$$

is invertible so $\dot{\boldsymbol{E}} \boldsymbol{E}^\dagger$ is uniquely determined in $\mathrm{stab}_{\boldsymbol{P}}^{\perp}$. In conclusion, we have derived the following result for the dynamics of $\boldsymbol{W}_s$ and $\boldsymbol{W}_r$.

THEOREM 3.2. *Let $\boldsymbol{W} = \boldsymbol{W}(t)$ and $\boldsymbol{P} = \boldsymbol{P}(t)$ be the vorticity and stream matrix for a solution to the Euler–Zeitlin equations (2.3a,b). Let $\boldsymbol{W}_s$ and $\boldsymbol{W}_r$ respectively be the*

orthogonal projections of $\boldsymbol{W}$ *onto* $stab_{\boldsymbol{P}}$ *and its orthogonal complement as in* (3.1). *Then* $\boldsymbol{W}_s$ *and* $\boldsymbol{W}_r$ *satisfy the following system of equations:*

$$\left.\begin{aligned}\dot{\boldsymbol{W}}_s &= [\boldsymbol{B}, \boldsymbol{W}_s] - \Pi_{\boldsymbol{P}}[\boldsymbol{B}, \boldsymbol{W}_r]\\ \dot{\boldsymbol{W}}_r &= -[\boldsymbol{B}, \boldsymbol{W}_s] + \Pi_{\boldsymbol{P}}[\boldsymbol{B}, \boldsymbol{W}_r] + [\boldsymbol{P}, \boldsymbol{W}_r],\end{aligned}\right\} \tag{3.17}$$

where $\boldsymbol{P} = \Delta_N^{-1}(\boldsymbol{W}_s + \boldsymbol{W}_r)$ *and* $\boldsymbol{B}$ *is the unique solution to*

$$[\boldsymbol{B}, \boldsymbol{P}] = \Pi_{\boldsymbol{P}}^{\perp}\Delta_N^{-1}[\boldsymbol{P}, \boldsymbol{W}_r], \quad \boldsymbol{B} \in stab_{\boldsymbol{P}}^{\perp}. \tag{3.18a,b}$$

From Theorem 3.2 we can deduce properties of $\boldsymbol{W}_s$ and $\boldsymbol{W}_r$. First, if $\boldsymbol{W}_r = 0$ then $\boldsymbol{B} \in \mathrm{stab}_{\boldsymbol{P}} \cap \mathrm{stab}_{\boldsymbol{P}}^{\perp}$ so $\boldsymbol{B} = 0$. Conversely, if $\boldsymbol{B} = 0$ then $\dot{\boldsymbol{W}}_s = 0$ and

$$\dot{\boldsymbol{W}}_r = [\Delta_N^{-1}(\boldsymbol{W}_s + \boldsymbol{W}_r), \boldsymbol{W}_r]. \tag{3.19}$$

Hence, in that case $\boldsymbol{W}_s$ plays the role of a fixed topography, and $\boldsymbol{W}_r$ satisfies the Euler–Zeitlin equation with forcing (3.19). From (3.18*a*,*b*) we deduce that $\boldsymbol{B} = 0$ also implies

$$\mathrm{Tr}(\Delta_N^{-1}\boldsymbol{W}_s[\Delta_N^{-1}\boldsymbol{W}_r, \boldsymbol{W}_r]) = 0. \tag{3.20}$$

Another observation is that if $[\boldsymbol{B}, \boldsymbol{W}_s] = 0$ then $\boldsymbol{B} = 0$ so $\dot{\boldsymbol{W}}_s = 0$. *Vice versa*, $\Pi_{\boldsymbol{P}}[\boldsymbol{B}, \boldsymbol{W}_r] = 0$ implies (3.20). This means that it is possible to have an evolution of the eigenvectors of P without any change of the eigenvalues, but not the other way around.

REMARK 3.3. *The projection* $\Pi_{\boldsymbol{P}}\colon \mathfrak{su}(N) \to stab_P$ *has rank* N *in the generic case. Hence, the dynamics of* $\boldsymbol{W}_s$ *in the moving frame* $\boldsymbol{E}_{kk}$ *can be described by only* N *components, namely its eigenvalues. Therefore, the vorticity splitting can be interpreted as a reduced dynamics. As we shall see in § 5 below, the projection* $\Pi_{\boldsymbol{P}}$ *is a quantised version of a mixing operator. Such operators were used by Shnirelman (1993) to characterise stationary flows.*

3.2. *Energy and enstrophy splitting*

We now study how the canonical splitting (3.1) couples with energy and enstrophy. Since $\mathrm{Tr}(\boldsymbol{P}\boldsymbol{W}_r) = 0$, the energy, given by the square of the energy norm, fulfils

$$\begin{aligned}H(\boldsymbol{W}) &= \tfrac{1}{2}\mathrm{Tr}(\boldsymbol{W}_s\Delta_N^{-1}(\boldsymbol{W}_s + \boldsymbol{W}_r))\\ &= \tfrac{1}{2}\mathrm{Tr}(\boldsymbol{W}_s\Delta_N^{-1}\boldsymbol{W}_s) - \tfrac{1}{2}\mathrm{Tr}(\boldsymbol{W}_r\Delta_N^{-1}\boldsymbol{W}_r).\end{aligned} \tag{3.21}$$

Yet, the enstrophy, corresponding to the enstrophy norm, fulfils

$$E(\boldsymbol{W}) = -\mathrm{Tr}(\boldsymbol{W}_s^2) - \mathrm{Tr}(\boldsymbol{W}_r^2). \tag{3.22}$$

These equalities furnish the interesting relations

$$\left.\begin{aligned}H(\boldsymbol{W}) &= H(\boldsymbol{W}_s) - H(\boldsymbol{W}_r)\\ E(\boldsymbol{W}) &= E(\boldsymbol{W}_s) + E(\boldsymbol{W}_r).\end{aligned}\right\} \tag{3.23}$$

Notice that $H(\boldsymbol{W}_s)$ is always larger than $H(\boldsymbol{W})$ and that the energies of $\boldsymbol{W}_s$ and $\boldsymbol{W}_r$ have to increase or decrease at the same rate. On the other hand, if the enstrophy of $\boldsymbol{W}_s$ decrease at some rate then the enstrophy of $\boldsymbol{W}_r$ must increase at the same rate. The canonical splitting

is thus coherent with Kraichnan's (1967) description of an inverse energy cascade and a forward enstrophy cascade.

The energy–enstrophy splitting (3.23) has a geometric interpretation. It says that $\boldsymbol{W}$ and $\boldsymbol{W}_r$ are orthogonal in the energy norm, whereas $\boldsymbol{W}_s$ and $\boldsymbol{W}_r$ are orthogonal in the enstrophy norm. Consider the plane spanned by $\boldsymbol{W}$ and $\boldsymbol{W}_r$, and let $H_r = H(\boldsymbol{W}_r)$ and $H_0 = H(\boldsymbol{W})$. Then, since $\boldsymbol{W}_r = (0, \sqrt{H_r})$ and $\boldsymbol{W} = (\sqrt{H_0}, 0)$ in this plane, energy corresponds to the Euclidean norm on $\mathbb{R}^2$. We want to express the enstrophy norm relative to the energy norm. First, observe that $\boldsymbol{W}_s = (\sqrt{H_0}, -\sqrt{H_r})$. The positive definite matrix $\boldsymbol{G}$ for the enstrophy inner product restricted to the $(\boldsymbol{W}, \boldsymbol{W}_r)$-plane can be written $\boldsymbol{G} = \boldsymbol{C}^\top \boldsymbol{C}$, where the matrix $\boldsymbol{C} \in \mathbb{R}^{2\times 2}$ is determined by $\boldsymbol{C} \cdot (0, \sqrt{H_r}) = (0, \sqrt{E_0} \sin\alpha)$ and $\boldsymbol{C} \cdot (\sqrt{H_0}, 0) = \sqrt{E_0}(\cos\alpha, \sin\alpha)$. Here, α is the angle between $\boldsymbol{W}$ and $\boldsymbol{W}_s$ in the enstrophy norm, and $E_0 = E(\boldsymbol{W})$. Then we have

$$\boldsymbol{G} = \begin{bmatrix} \dfrac{E_0}{H_0} & \dfrac{E_0}{\sqrt{H_r}\sqrt{H_0}} \sin^2\alpha \\ \dfrac{E_0}{\sqrt{H_r}\sqrt{H_0}} \sin^2\alpha & \dfrac{E_0}{H_r} \sin^2\alpha \end{bmatrix}. \tag{3.24}$$

PROPOSITION 3.4. *Let* $\boldsymbol{W} \neq 0$. *Then*

$$0 < H(\boldsymbol{W}) \leqslant H(\boldsymbol{W}_s) < E(\boldsymbol{W}_s) \leqslant E(\boldsymbol{W}). \tag{3.25}$$

Moreover, with notation as above

$$\left.\begin{aligned} H_r &\leqslant E_r = E_0 \sin^2\alpha \\ N^2 H_r &\geqslant E_r = E_0 \sin^2\alpha. \end{aligned}\right\} \tag{3.26}$$

Hence, if $\sin\alpha \neq 0$ *then*

$$\frac{E_0}{N^2} \leqslant \frac{H_r}{\sin^2\alpha} \leqslant E_0. \tag{3.27}$$

Proof. First notice that $\boldsymbol{W}_s = 0$ if and only if $\boldsymbol{W} = 0$ since $\sqrt{H(\cdot)}$ is a norm. The inequalities (3.25) then follow from (3.23) and the fact that the enstrophy is always larger than the energy. To get the second inequality of (3.26), we use that the largest eigenvalue of the discrete Laplacian Δ_N is $(N-1)N$. ∎

REMARK 3.5. *In the limit* $N \to \infty$ *the ratio* $\sin^2\alpha / H_r$ *in* (3.27) *is potentially unbounded. It could, and does, happen that the enstrophy norm of* $\boldsymbol{W}_r$ *is far from zero while its energy norm tends to zero. This corresponds to* $\boldsymbol{W}_r$ *being shifted towards small scales while not decreasing in enstrophy. It is a manifestation of Kraichnan's theory of forward enstrophy and inverse energy cascades.*

4. Dynamically emerging scale separation

This section contains numerical evidence that the canonical vorticity splitting (3.1) captures the dynamics of scale separation. We also provide theoretical arguments to support these results. To give a complete mathematical proof that fully explains the numerical observations is a challenge not addressed in this paper.

A good reason to study the vorticity splitting $\boldsymbol{W} = \boldsymbol{W}_s + \boldsymbol{W}_r$ is that unsteadiness precisely means non-vanishing of $\boldsymbol{W}_r$. From an analytical point of view, $\boldsymbol{W}_s$ represents

a projection of $\boldsymbol{W}$ onto a smoother subspace. Indeed, the relation via the Laplace operator between $\boldsymbol{P}$ and $\boldsymbol{W}$ says that $\boldsymbol{P}$ admits two derivatives more than $\boldsymbol{W}$ does. Hence, since $\boldsymbol{W}_s$ is related to $\boldsymbol{P}$ via a polynomial relationship, $\boldsymbol{W}_s$ is, in general, more regular than $\boldsymbol{W}$. *Vice versa*, $\boldsymbol{W}_r$ contains the rougher part of $\boldsymbol{W}$. The tempting conjecture is that $\boldsymbol{W}_s$ represents the low-dimensional, large-scale dynamics, whereas $\boldsymbol{W}_r$ represents the noisy, small-scale dynamics. To assess this conjecture we present two numerical simulations, both with randomly generated, smooth initial data. These two simulations represent the two generic behaviours described by Modin & Viviani (2020*a*): formation of either 3 or 4 coherent vortex formations, strongly correlated to the momentum–enstrophy ratio. (We have run many more simulation with randomly generated initial conditions. The two simulations presented here capture the universal behaviour in all simulations.)

4.1. *Vanishing momentum simulation*

This simulation starts from smooth, randomly generated initial data. Each spherical harmonic coefficient ω^{lm} in the range $2 \leqslant l \leqslant 10$ was drawn from the standard normal distribution. The remaining coefficients were set to zero. The data were then transformed to a vorticity matrix of size $N = 512$ (see Modin & Viviani (2020*a*) for details and explicit formulae). For reproducibility, the initial conditions are available in the supplementary material at https://doi.org/10.1017/jfm.2022.457.

For time discretisation of the Euler–Zeitlin equations (2.3*a*,*b*) we use the second-order isospectral midpoint method (Modin & Viviani 2020*b*). The time step length is 1.2239×10^{-4} s. This corresponds to 0.2 time units in Zeitlin's model, which scales time by $4\sqrt{\pi}/N^{3/2}$.

To visualise the fluid motion stages, we sample at the initial time ($t = 0$), at an intermediate time during mixing ($t = 13$ s) and at a long time well after the large-scale condensates are formed ($t = 318$ s). The vorticity matrices at these outputs are then transformed to functions in azimuth–elevation coordinates. The result is shown in figure 1.

Due to vanishing momentum ($\omega^{1m} = 0$ in the initial data), integrability theory for the Hamiltonian dynamics on the sphere suggests that 4 vortex blobs should appear (Modin & Viviani 2020*a*,*b*). Indeed they do appear and then pass into quasi-periodic orbits. The first movie of the supplementary material captures the entire process. On top of the large-scale condensates, a noisy, fine-scale structure emerges. In essence, we see a separation of scales.

Figure 2 displays azimuth–elevation fields for the stream matrix $\boldsymbol{P}$ and the vorticity matrix components $\boldsymbol{W}_s$ and $\boldsymbol{W}_r$ at the same sampled output times. After some time of initial mixing, the large scales of the vorticity are all contained in $\boldsymbol{W}_s$, whereas $\boldsymbol{W}_r$ collects the small-scale fluctuations. The long-time $\boldsymbol{W}_r$ state resembles noise but, as such, is not completely uniform. In fact, the non-uniform character captures the quasi-periodic dynamics since $\dot{\boldsymbol{W}} = [\boldsymbol{P}, \boldsymbol{W}_r]$. An open problem is to model the noise by a stochastic process.

Figure 3 shows the evolution of the energy and enstrophy of $\boldsymbol{W}_s$ and $\boldsymbol{W}_r$. Over time, E_r increases whereas H_r decreases. Also notice that E_s, E_r, H_s and H_r fulfil the energy and enstrophy relations (3.23). The residual vorticity $\boldsymbol{W}_r$ decreases in energy norm but increases in enstrophy norm. This is a quantification of Kraichnan's (1967) qualitative description.

The scale separation of the vorticity is even more clear in the spectral domain. Figure 4 contains energy spectra for $\boldsymbol{W}$, $\boldsymbol{W}_s$ and $\boldsymbol{W}_r$ at the sampled output times. The energy level $H(l)$, corresponding to the wavenumber $l = 1, \ldots, N$, contains the energy of the modes

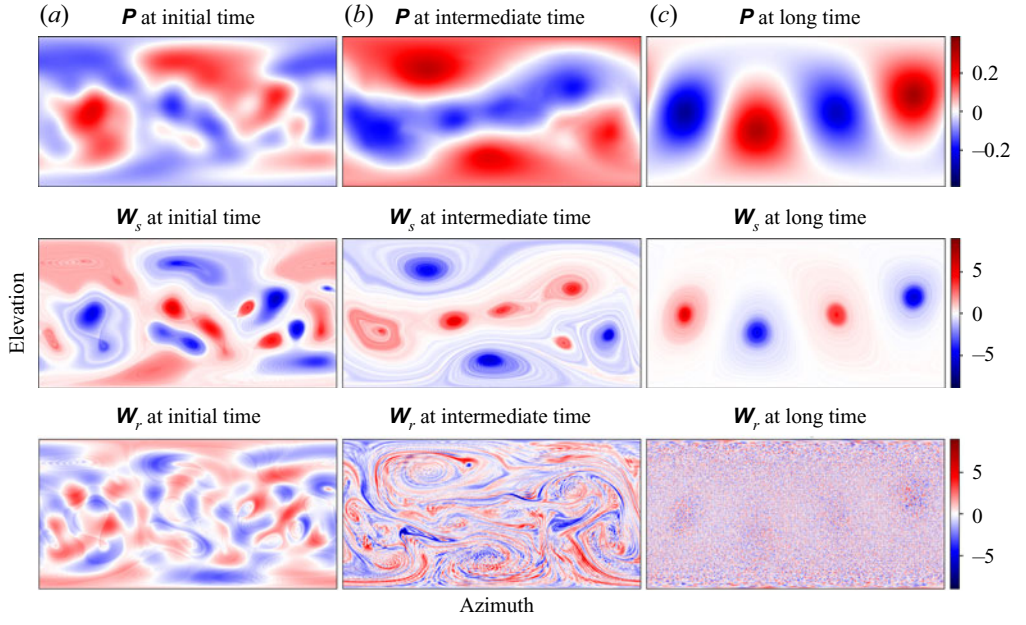

Figure 2. Vanishing momentum simulation. Progression of the stream matrix $\boldsymbol{P}$ and the components $\boldsymbol{W}_s$ and $\boldsymbol{W}_r$ for the same simulation as in figure 1. Initially, $\boldsymbol{W}_s$ and $\boldsymbol{W}_r$ are similar in nature, but they evolve so $\boldsymbol{W}_s$ traps the large-scale condensates whereas $\boldsymbol{W}_r$ captures the small-scale fluctuations.

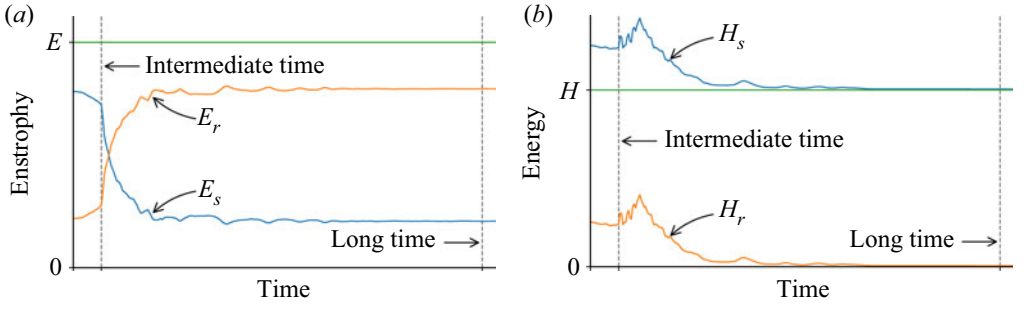

Figure 3. Vanishing momentum simulation. Evolution of the decomposed enstrophies E_s and E_r (a), and decomposed energies H_s and H_r (b). The dashed, vertical lines indicate the sample times in figures 1, 2 and 4. The energy H_r decays almost to zero so that most of the energy is contained in H_s (reflecting the inverse energy cascade). On the other hand, the enstrophy E_r increases over time (reflecting the forward enstrophy cascade).

for the spherical harmonics Y_{lm} with $m = -l, \ldots, l$. We notice that the energy spectrum of $\boldsymbol{W}$ is similar in nature to that described by Boffetta & Ecke (2012). Indeed, the 'broken line' slope in the energy spectrum of $\boldsymbol{W}$ originates from an l^{-3} slope of $\boldsymbol{W}_s$ and an l^{-1} slope of $\boldsymbol{W}_r$. Thus, the vorticity splitting yields a scale separation of the vorticity field that exactly reflects the broken line spectra previously observed in numerical simulations and empirical observations. The broken line spectrum is not reached at the intermediate time before mixing has settled.

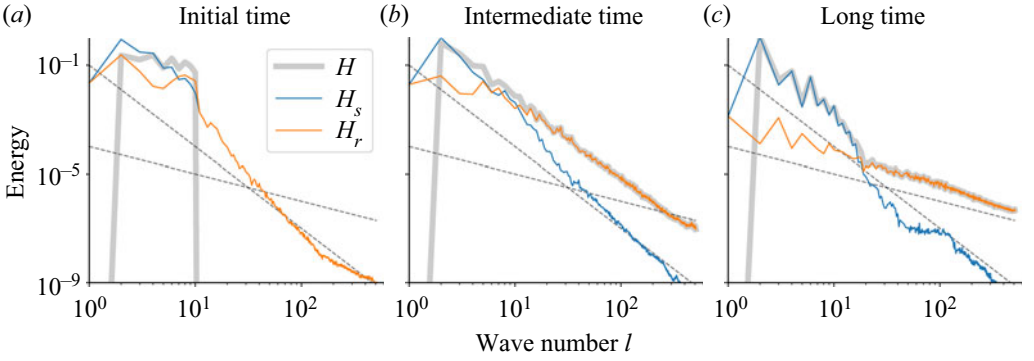

Figure 4. Vanishing momentum simulation. Spectrum in log–log scale for the energies H, H_s and H_r at the initial (a), intermediate (b) and long times (c). The dashed lines indicate the slopes l^{-3} and l^{-1}. The slope of H_s is almost settled at the intermediate time. The slope of H_r takes much longer to settle. At long times, the broken line spectrum of H is captured well by the components H_s and H_r, which themselves have almost the same average slope at each scale.

4.2. *Non-vanishing momentum simulation*

In this simulation, the initial data were generated much like before, but now the range of non-zero spherical harmonics coefficients ω^{lm} is $1 \leqslant l \leqslant 10$. Consequently, the total angular momentum is no longer zero. For reproducibility also of this simulation, the generated initial conditions are available in the supplementary material. Time discretisation, step size lengths, etc. are selected as in the previous simulation.

Figure 5 shows azimuth–elevation fields corresponding to the stream matrix $\boldsymbol{P}$, the vorticity matrix $\boldsymbol{W}$ and the components $\boldsymbol{W}_s$ and $\boldsymbol{W}_r$, sampled at initial time ($t = 0$), intermediate time ($t = 13$ s) and long time ($t = 344$ s). The entire motion is captured in the second movie of the supplementary material. Three vortex blobs emerge. The formation of these, from initial data with non-vanishing momentum, is again predicted and demonstrated by Modin & Viviani (2020*a*). It reflects the integrability of the low-dimensional Hamiltonian dynamics on the sphere. As before, the large-scale vorticity patterns are contained in the $\boldsymbol{W}_s$ component. The $\boldsymbol{W}_r$ component swiftly develops noisy fluctuations. At long times, it is less uniform than in the vanishing momentum simulation. The reason is that the 3 blobs here move faster than the 4 blobs in the previous simulation.

The scale separation of the vorticity is again evident from the energy spectrum of $\boldsymbol{W}$. Figure 6 gives energy spectra for the three vorticity fields $\boldsymbol{W}$, $\boldsymbol{W}_s$ and $\boldsymbol{W}_r$. The results are analogous to those in figure 4.

4.3. *Streamfunction–vorticity branching and blobs*

In the literature on 2-D turbulence, steady solutions are often characterised by a functional relation between the streamfunction and vorticity. Branching in such relations has been used as a measure of unsteadiness (Dritschel *et al.* 2015).

Since $\boldsymbol{W} = \boldsymbol{W}_s$ if and only if $\boldsymbol{W}$ is a steady solution, it is natural to consider scatter plots between values of $\boldsymbol{P}$ and $\boldsymbol{W}_s$. Such diagrams are given at the initial, intermediate and long times, in figure 7 for the vanishing momentum simulation, and in figure 8 for the non-vanishing momentum simulation. The following interpretation of branches is more fundamental than interpretations related to unsteadiness. Each branch represents and characterises a specific blob in $\boldsymbol{W}_s$. Upward branches represent blobs with positive values.

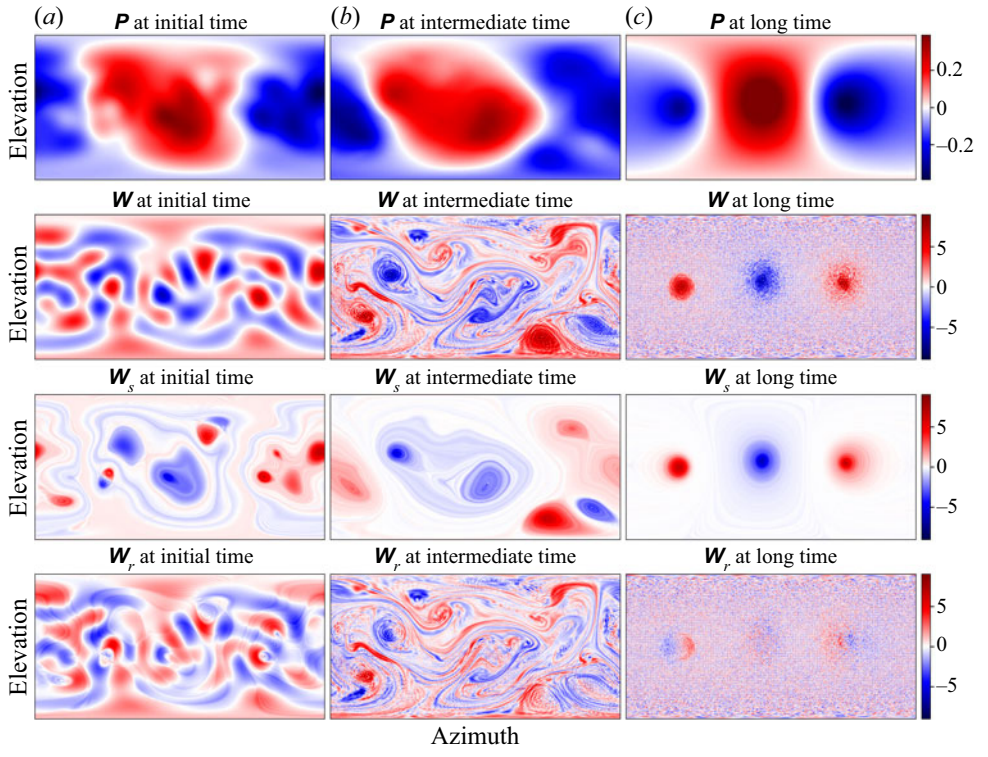

Figure 5. Non-vanishing momentum simulation. Progression of the stream matrix $\boldsymbol{P}$ and the components $\boldsymbol{W}_s$ and $\boldsymbol{W}_r$ of the vorticity matrix $\boldsymbol{W}$. Initially, $\boldsymbol{W}_s$ and $\boldsymbol{W}_r$ are similar in nature, but they evolve so that $\boldsymbol{W}_s$ contains the large-scale condensates whereas $\boldsymbol{W}_r$ contains the small-scale fluctuations.

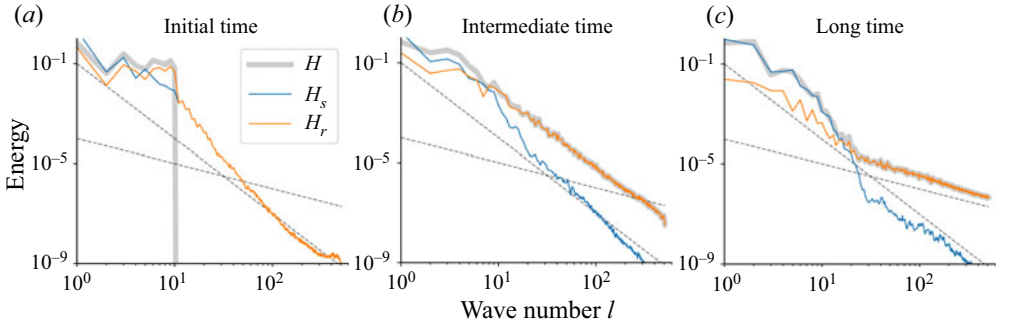

Figure 6. Non-vanishing momentum simulation. Spectrum in log–log scale for the energies H, H_s and H_r at the initial (a), intermediate (b) and long times (c). The dashed lines indicate the slopes l^{-3} and l^{-1}. The slope of H_s is almost settled at the intermediate time. The slope of H_r takes much longer to settle. At long times, the broken line spectrum of H is captured well by the components H_s and H_r, which themselves have almost the same average slope at each scale.

Vice versa for downward branches. This is particularly clear at the long times, where there are fewer blobs. However, the interpretation is valid also at the initial and intermediated times, as revealed by carefully comparing the branching diagrams with the values of $\boldsymbol{P}$ and $\boldsymbol{W}_s$ in figures 2 and 5. The end of each specific branch (sometimes they overlap) is then readily identified with a specific blob. The steepness of the branch corresponds to $\mathrm{d}\boldsymbol{W}_s/\mathrm{d}\boldsymbol{P}$.

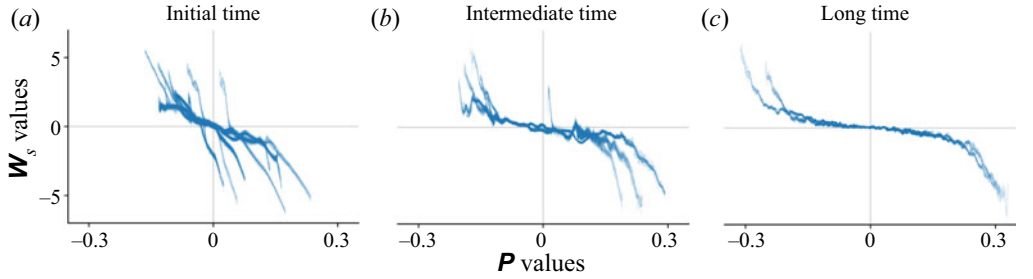

Figure 7. Vanishing momentum simulation. Values of $\boldsymbol{P}$ vs values of $\boldsymbol{W}_s$. The end of each branch corresponds to a blob in the $\boldsymbol{W}_s$ plot in figure 2. Upward if the blob is positive, otherwise downward. For example, at intermediate time, the sharp upward branch close to the y-axis matches the small positive blob of $\boldsymbol{W}_s$ in the lower-right corner of the corresponding plot in figure 2.

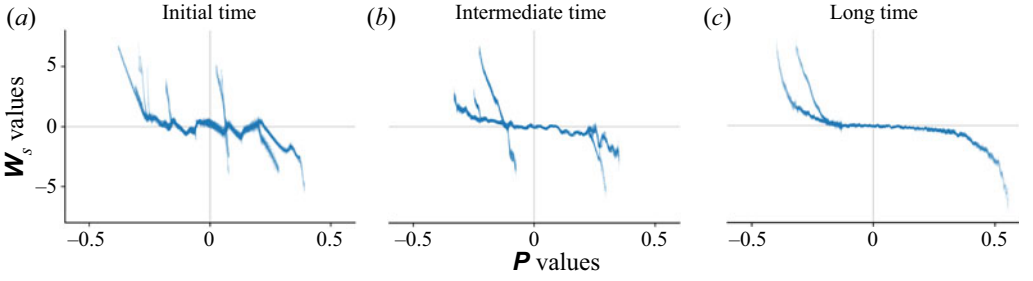

Figure 8. Non-vanishing momentum simulation. Values of $\boldsymbol{P}$ vs values of $\boldsymbol{W}_s$. The end of each branch corresponds to a blob in figure 5. For example, at the initial time, a careful study reveals that the steep, overlapping branches just to the right of the y-axis match the two positive–negative blob pairs seen in the corresponding plot in figure 5.

This can be used to determine the shape of the blob, assuming axisymmetry. For example, in figure 8 at long times, the steeper of the two upward branches corresponds to the left-most, sharper of the two positive blobs in figure 5. The two negative blobs at long times in figure 2 are almost indistinguishable, which is reflected as overlapping downward branches in figure 7.

5. Canonical splitting of the vorticity function

In this section, we map our results for the Euler–Zeitlin equations to the original Euler equations (1.1*a*,*b*). Indeed, all the concepts needed in the canonical splitting for the Euler–Zeitlin equations have classical counterparts; some are listed in table 1. However, one has to be careful to rigorously define these concepts: the transition from the quantised to the classical equations is valid only in a weak sense. Mathematically, the correct framework is L^∞ weak-star convergence. Formally, we may nevertheless proceed as follows, keeping in mind that concepts are transferable only in the weak sense. The key ingredient is that the projection $\Pi_{\boldsymbol{P}}$ onto the stabiliser of $\boldsymbol{P}$ corresponds to averaging along the level sets of the streamfunction ψ. This gives the canonical splitting for the vorticity function via the projector Π_ψ as

$$\omega = \Pi_\psi(\omega) + \Pi_\psi^\perp(\omega) = \omega_s + \omega_r. \tag{5.1}$$

The projection Π_ψ is time dependent, since the level curves of ψ change with time.

	Euler's equations	Zeitlin's model
Lie group	Symplectic diffeomorphisms	$\mathrm{SU}(N)$
Lie algebra	Divergence free vector fields	$\mathfrak{su}(N)$
Phase space	L^∞ functions	$\mathfrak{su}(N)^* \simeq \mathfrak{su}(N)$
Strong norm	Supremum norm $\|\cdot\|_{L^\infty}$	Spectral norm
Energy norm	Sobolev norm $\|\cdot\|_{H^{-1}}$	$\sqrt{-\operatorname{Tr}(\boldsymbol{PW})}$
Enstrophy norm	L^2 norm $\|\cdot\|_{L^2}$	Frobenius norm
Canonical splitting	Averaging on level-sets of ψ	Projection onto stabiliser of $\boldsymbol{P}$
z-axis symmetry	ω is zonal	$\boldsymbol{W}$ is diagonal

Table 1. Dictionary between Euler's and Zeitlin's models of hydrodynamics.

Let us now proceed with more mathematical details on this construction. First, recall again Euler's equations in vorticity formulation

$$\dot{\omega} = \{\psi, \omega\}, \quad \Delta\psi = \omega. \tag{5.2a,b}$$

To define the continuous analogue of the vorticity matrix splitting, we have to understand equations (5.2a,b) in the weak sense. Indeed, in general, the projections Π_ψ and $\Pi_\psi^\perp$ cannot preserve the smoothness of ω. But for any $p \in [1, \infty]$ they are continuous operators from $C^0(\mathbb{S}^2)$ to $L^p(\mathbb{S}^2)$ with operator norm one. Since continuous functions are dense in $L^p(\mathbb{S}^2)$, we can extend Π_ψ and $\Pi_\psi^\perp$ to continuous operators on $L^\infty(\mathbb{S}^2)$. This result fits well with the global well posedness of (5.2a,b), which precisely requires a vorticity function in L^∞ (Yudovich 1963; Majda & Bertozzi 2002; Marchioro & Pulvirenti 2012).

Let us first give (5.2a,b) in the weak sense. For any $p \geqslant 2$, if $\omega \in L^p(\mathbb{S}^2)$ then $\psi \in W^{2,p}(\mathbb{S}^2) \subset H^1(\mathbb{S}^2)$. We define the weak Poisson bracket as

$$\int_{\mathbb{S}^2} \{\psi, \omega\}\phi = -\int_{\mathbb{S}^2} \omega\{\psi, \phi\}, \tag{5.3}$$

for any test function $\phi \in C^\infty(\mathbb{S}^2)$. Hence, we define the stabiliser of ψ as

$$\mathrm{stab}_\psi := \{f \in L^2(\mathbb{S}^2) \mid \{f, \psi\} = 0\}. \tag{5.4}$$

Next, we define the L^2 orthogonal projection Π_ψ onto stab_ψ.

PROPOSITION 5.1. *If $p \geqslant 2$ and $\psi \in W^{2,p}(\mathbb{S}^2)$ then stab_ψ is a closed subspace of $L^2(\mathbb{S}^2)$.*

Proof. Let $\{f_n\} \subset \mathrm{stab}_\psi$, such that $f_n \to f$ in L^2, for $n \to \infty$. We want to show that $f \in \mathrm{stab}_\psi$. Let ϕ be a function in $C^1(\mathbb{S}^2)$, then we get

$$\left|\int \{f, \psi\}\phi\right| = \left|\int \{\phi, \psi\}f\right| = \left|\int \{\phi, \psi\}(f - f_n)\right| \leqslant \|\{\phi, \psi\}\|_0 \|f - f_n\|_0 \to 0, \tag{5.5}$$

for $n \to \infty$. ∎

The operator Π_ψ has an explicit form when evaluated on continuous functions. To state it, we first make the following assumption on the critical points of ψ.

ASSUMPTION 5.2. *Let $\psi \in C^1(\mathbb{S}^2)$ be the streamfunction. Then the critical points of ψ define a set of zero Lebesgue measure on $\mathbb{S}^2$, such that it is never dense in any neighbourhood of one of its points.*

We say that ψ is generic whenever it satisfies Assumption 5.2. Consider now some $f \in C^1(\mathbb{S}^2)$. Then $f \in \mathrm{stab}_\psi$ if and only ∇f and $\nabla \psi$ are parallel. Since we take ψ to be generic, the points where $\{\boldsymbol{x} \mid \nabla \psi(\boldsymbol{x}) = 0\}$ lie on a set of zero measure, nowhere dense. Therefore, since f is continuous, $f \in \mathrm{stab}_\psi$ if it is constant on the connected components of the level curves of ψ. Then the projection of f onto stab_ψ can be defined by evaluating f on the level curves of ψ, i.e. the streamlines. Let $\boldsymbol{\gamma}$ be a connected component of a streamline, then define the projection $\Pi_\psi : C^1(\mathbb{S}^2) \to \mathrm{stab}_\psi$ as

$$\Pi_\psi(f)\big|_{\boldsymbol{\gamma}} = \frac{1}{\mathrm{length}(\boldsymbol{\gamma})} \int_{\boldsymbol{\gamma}} f \, \mathrm{d}s. \tag{5.6}$$

In the limit when $\boldsymbol{\gamma}$ approaches a single point, clearly $\Pi_\psi(\omega)_{|\boldsymbol{\gamma}} = f(\boldsymbol{\gamma})$.

The operator Π_ψ does not, in general, preserve the continuity of f. Indeed, consider a bifurcation saddle point $\boldsymbol{x} \in \mathbb{S}^2$, namely a saddle point of ψ such that the streamline passing through x contains a bifurcation point. We then have the following result.

PROPOSITION 5.3. *Let ψ be generic and Π_ψ the projection defined in (5.6). If $\boldsymbol{x} \in \mathbb{S}^2$ is a bifurcation saddle point for ψ, then there exists $f \in C^1(\mathbb{S}^2)$ such that $\Pi_\psi(f)$ is discontinuous at the streamline passing through $\boldsymbol{x}$. Vice versa, given $f \in C^1(\mathbb{S}^2)$, if $\Pi_\psi(f)$ is discontinuous at some point $\boldsymbol{x} \in \mathbb{S}^2$, then the streamline passing through $\boldsymbol{x}$ contains a bifurcation saddle point.*

Proof. (Sketch) The issue about the continuity of f can be treated locally. Hence, let us work in Cartesian coordinates. Let $\boldsymbol{x} \in \mathbb{S}^2$ be a bifurcation saddle point for ψ and $\boldsymbol{\gamma}$ the streamline passing through $\boldsymbol{x}$. Then, let β be a curve intersecting $\boldsymbol{\gamma}$ only in $\boldsymbol{x}$ and let f be a smooth function positive at one side of β and negative at the other one, such that $\int_{\boldsymbol{\gamma}} f \, \mathrm{d}s = 0$. Then, with $\boldsymbol{x}$ a bifurcation point, for any neighbourhood U of $\boldsymbol{x}$, there exist streamlines totally contained in one or another side of β. Then, the average of f on those streamlines is either strictly positive or negative, creating a discontinuity at $\boldsymbol{\gamma}$.

Vice versa, let $f \in C^1(\mathbb{S}^2)$, such that $\Pi_\psi(f)$ is discontinuous at some point $\boldsymbol{x} \in \mathbb{S}^2$. Then, the streamline passing through x cannot be homeomorphic to any of those in some tubular neighbourhood. Hence, the streamline passing through $\boldsymbol{x}$ must contain a critical point for ψ, which also is a bifurcation saddle point. ∎

However, we have the following regularity for Π_ψ.

PROPOSITION 5.4. *For any $p \in [1, \infty]$, the operator Π_ψ can be extended to a bounded operator with norm one on $L^p(\mathbb{S}^2)$.*

Proof. Let us first notice that Π_ψ is defined from $C^0(\mathbb{S}^2)$ to $L^1(\mathbb{S}^2)$, and satisfies $\|\Pi_\psi f\|_{L^1} \leqslant \|f\|_{L^1}$, for any $f \in C^0(\mathbb{S}^2)$. Since $C^0(\mathbb{S}^2)$ is dense in $L^1(\mathbb{S}^2)$, it is possible to extend Π_ψ to a bounded operator on $L^1(\mathbb{S}^2)$. Secondly, Π_ψ is well defined from the space of simple functions to $L^\infty(\mathbb{S}^2)$, and satisfies $\|\Pi_\psi f\|_{L^\infty} \leqslant \|f\|_{L^\infty}$, for any f simple. Since the space of simple functions is dense in $L^\infty(\mathbb{S}^2)$, it is possible to extend Π_ψ to a bounded operator on $L^\infty(\mathbb{S}^2)$. Furthermore, since Π_ψ fixes the constant functions, it must

be that $\|\Pi_\psi\|_{L^1} = \|\Pi_\psi\|_{L^\infty} = 1$. Hence, by the Riesz–Thorin theorem, we conclude that $\|\Pi_\psi\|_{L^p} = 1$, for any $p \in [1, \infty]$. ∎

Hence, from now on, let us consider (5.2*a*,*b*) in the weak form, for $\omega \in L^\infty(\mathbb{S}^2)$. It is clear that $\Pi_\psi^2 = \Pi_\psi$. Moreover, we can formally define the operator Π_ψ via the kernel

$$K(\boldsymbol{x}, \boldsymbol{y}) = \frac{1}{\text{length}(\boldsymbol{\gamma}_{\boldsymbol{x}})} \delta_{\boldsymbol{\gamma}_{\boldsymbol{x}}}(\boldsymbol{y}), \quad \text{for any } \boldsymbol{x}, \boldsymbol{y} \in \mathbb{S}^2 \tag{5.7}$$

where $\boldsymbol{\gamma}_{\boldsymbol{x}}$ is the connected component of the streamline passing through $\boldsymbol{x}$. In this way we get that Π_ψ is self-adjoint with respect to the L^2 inner product, i.e. for any $f, g \in C^\infty(\mathbb{S}^2)$

$$\begin{aligned} \int_{\mathbb{S}^2} f \Pi_\psi g &= \int_{\mathbb{S}^2} f(\boldsymbol{x}) \int_{\mathbb{S}^2} K(\boldsymbol{x}, \boldsymbol{y}) g(\boldsymbol{y}) \\ &= \int_{\mathbb{S}^2} g(\boldsymbol{y}) \int_{\mathbb{S}^2} K(\boldsymbol{x}, \boldsymbol{y}) f(\boldsymbol{x}) \\ &= \int_{\mathbb{S}^2} g \Pi_\psi f. \end{aligned} \tag{5.8}$$

By extension these equalities are valid for $f, g \in L^p(\mathbb{S}^2)$ whenever $p \in [1, \infty]$.

REMARK 5.5. *We notice that the operator Π_ψ, defined by the kernel $K(\boldsymbol{x}, \boldsymbol{y})$, is a mixing operator (or polymorphism or bistochastic operator), as introduced by Shnirelman (1993, 2013). Such operators give rise to a partial ordering on $L^2(\mathbb{S}^2)$: for any $f, g \in L^2(\mathbb{S}^2)$, $f \dashv g$ if there exists a mixing operator, defined via the kernel K, such that $f = K * g$. In his work, Shnirelman shows that stationary flows are characterised as minimal elements of this ordering. In a way, our work shows that it is enough to consider mixing operators of the form Π_ψ. Within this class, ω is minimal if there exists a streamfunction such that $\Pi_\psi \omega = \omega$. As we see next, this in turn implies that ω is stationary.*

PROPOSITION 5.6. *Let $\psi \in C^1(\mathbb{S}^2)$ be generic. For $\omega \in L^\infty(\mathbb{S}^2)$ we then have*

$$\omega \in \mathit{stab}_\psi \iff \Pi_\psi \omega = \omega. \tag{5.9}$$

Proof. We prove the result for $\omega \in C^1(\mathbb{S}^2)$, then conclude by extension. Let $\omega \in \text{stab}_\psi$. Then, $\nabla\omega$ is parallel to $\nabla\psi$ almost everywhere. Hence, the gradient of ω along any streamline must vanish, and so on each connected component it is constant. By continuity of ω we deduce that f must be constant also on the streamlines containing critical points. Therefore, $\Pi_\psi \omega = \omega$. Assume now that $\Pi_\psi \omega = \omega$. Then ω must be constant on each connected component of a streamline. Hence, $\nabla\omega$ is orthogonal to the streamlines. Since $\nabla\psi$ is also orthogonal to the streamlines, we conclude that $\{\omega, \psi\} = 0$, i.e. $\omega \in \text{stab}_\psi$. ∎

We are now in the position to derive continuous analogues of the results in § 3 (which, remember, are based on Lie theory for matrices). First, the streamfunction ψ satisfies the

equation

$$\dot{\psi} = \Delta^{-1}\{\psi, \Delta\psi\}. \tag{5.10}$$

This equation is not Hamiltonian. But we can split the right-hand side into a Hamiltonian and non-Hamiltonian part via the projection Π_ψ

$$\dot{\psi} = \Pi_\psi^\perp \Delta^{-1}\{\psi, \Delta\psi\} + \Pi_\psi \Delta^{-1}\{\psi, \Delta\psi\}. \tag{5.11}$$

Analogous to the quantised case, we seek a generator for $\Pi_\psi^\perp \Delta^{-1}\{\psi, \Delta\psi\}$. That is, a function $b\colon \mathbb{S}^2 \to \mathbb{R}$ such that

$$\{b, \psi\} = \Pi_\psi^\perp \Delta^{-1}\{\psi, \Delta\psi\}. \tag{5.12}$$

It is clear that a necessary condition for the equation $\{b, \psi\} = f$ to have a solution b is that $f \in \mathrm{stab}_\psi^\perp$. Indeed, if $b \in C^1(\mathbb{S}^2)$ then $\{b, \psi\} \in \mathrm{stab}_\psi^\perp$ since

$$\int_{\mathbb{S}^2} \{b, \psi\} g = -\int_{\mathbb{S}^2} \{g, \psi\} b = 0 \quad \text{for any } g \in \mathrm{stab}_\psi. \tag{5.13}$$

However, in general (5.12) can be solved only where $\nabla\psi \neq 0$. Around the critical points of ψ the gradient of b is potentially unbounded. Moreover, the right-hand side in (5.12) can be discontinuous at the level curves of ψ containing saddle points of ψ. Hence, b can only be defined almost everywhere. Furthermore, we have the following:

PROPOSITION 5.7. *Let $f \in C^0(\mathbb{S}^2)$ and ψ be generic. Then $f \in \mathrm{stab}_\psi^\perp$ if and only if there exists b almost everywhere smooth, such that $\{b, \psi\} = f$ on the set $\nabla\psi \neq 0$.*

Proof. The if part is clear. Let instead take $f \in \mathrm{stab}_\psi^\perp$. Then, for any point $\boldsymbol{x} \in \mathbb{S}^2$, we have to solve the partial differential equation (PDE) for b

$$\nabla^\perp\psi \cdot \nabla b = f, \tag{5.14}$$

where $\nabla^\perp\psi = \boldsymbol{x} \times \nabla\psi$. If $\nabla\psi$ does not vanish, (5.14) can be solved by integration in the direction of $\nabla^\perp\psi$. At the points where $\nabla\psi$ does not vanish, ∇b is not defined by (5.14), and it can be unbounded around those points. Hence, the field b is almost everywhere smooth and satisfies $\{b, \psi\} = f$, where $\nabla\psi \neq 0$. ∎

5.1. *Dynamics of ω_s and ω_r*

To derive the dynamical equations for ω_s, we cannot directly define the field b corresponding to the quantised field B above. Instead, we consider the volume-preserving vector field

$$X[\psi] := \Pi_\psi^\perp \Delta^{-1}\{\psi, \Delta\psi\}. \tag{5.15}$$

We note that X corresponds to the infinitesimal action of a map φ_t which transports ψ by deforming its level curves. Hence, φ_t acts naturally on stab_ψ. Let us write Π_ψ^t for the

projection onto stab_ψ at time t. Then, for any point $\boldsymbol{x} \in \mathbb{S}^2$, let

$$\boldsymbol{\gamma}(t) = \{\boldsymbol{y} \mid \psi(\boldsymbol{y}) = \psi(\boldsymbol{x}) \text{ and } \boldsymbol{y} \text{ in connected component of } \boldsymbol{x}\}, \tag{5.16}$$

and $\mathrm{d}\widehat{s_t}$ be the normalised Lebesgue measure on $\gamma(t)$. We have then the formal identity

$$\begin{aligned}\omega_s(t,\boldsymbol{x}) &= \varPi_\psi^t \omega(t,\boldsymbol{x}) \\ &= \int_{\boldsymbol{\gamma}(t)} \omega(t,\boldsymbol{y})\,\mathrm{d}\widehat{s_t}(\boldsymbol{y}) \\ &= \int_{\boldsymbol{\gamma}(0)} (\varphi_t^*\omega)(t,\boldsymbol{y})\,\mathrm{d}\widehat{s_0}(\boldsymbol{y}) \\ &= \varPi_\psi^0(\varphi_t^*\omega)(t,\varphi_t^{-1}(x)).\end{aligned} \tag{5.17}$$

Hence, for any test function $\phi \in C^\infty(\mathbb{S}^2)$

$$\begin{aligned}\frac{\mathrm{d}}{\mathrm{d}t}\int_{\mathbb{S}^2} \omega_s(t,\boldsymbol{x})\phi(\boldsymbol{x}) &= \frac{\mathrm{d}}{\mathrm{d}t}\int_{\mathbb{S}^2} \varPi_\psi^0(\varphi_t^*\omega)(t,\varphi_t^{-1}(\boldsymbol{x}))\phi(\boldsymbol{x}) \\ &= \int_{\mathbb{S}^2} \left(\varPi_\psi^0(\varphi_t^*\mathcal{L}_X\omega)(t,\varphi_t^{-1}\boldsymbol{x}) - \mathcal{L}_X\varPi_\psi^0(\varphi_t^*\omega)(t,\varphi_t^{-1}\boldsymbol{x})\right)\phi(\boldsymbol{x}) \\ &= -\int_{\mathbb{S}^2} \omega(t,\boldsymbol{x})\mathcal{L}_X\varPi_\psi^t\phi(\boldsymbol{x}) + \mathcal{L}_X\varPi_\psi^t\omega(t,\boldsymbol{x})\phi(\boldsymbol{x}),\end{aligned} \tag{5.18}$$

where $\mathcal{L}_X$ is the Lie derivative, which simply acts on functions as $\mathcal{L}_X f = X[f]$. We notice from the previous calculations that $\mathcal{L}_X$ has to be evaluated only on elements in stab_ψ. Hence, the time derivative of ω_s is well defined in the weak sense.

Let us now formally denote $X := -\{b, \cdot\}$. Then, interpreting the Poisson bracket in the weak sense, we can write the dynamical system for ω_s and ω_r as

$$\left.\begin{aligned}\dot{\omega}_s &= \{b,\omega_s\} - \varPi_\psi\{b,\omega_r\} \\ \dot{\omega}_r &= -\{b,\omega_s\} + \varPi_\psi\{b,\omega_r\} + \{\psi,\omega_r\} \\ \{b,\psi\} &= \varPi_\psi^\perp \varDelta^{-1}\{\psi,\omega_r\},\end{aligned}\right\} \tag{5.19}$$

where b is implicitly defined by the third equation and $\psi = \varDelta^{-1}(\omega_s + \omega_r)$. We notice that the equations of motion for ω_s can also be written in a more compact form as

$$\dot{\omega}_s = [\varPi_\psi, \mathcal{L}_X]\omega, \tag{5.20}$$

where the square bracket is the commutator of operators.

Finally, notice that the energy and enstrophy splitting is valid also in the classical setting

$$\left.\begin{aligned}H(\omega) &= H(\omega_s) - H(\omega_r) \\ E(\omega) &= E(\omega_s) + E(\omega_r).\end{aligned}\right\} \tag{5.21}$$

6. Conclusions and outlook

Based on the Euler–Zeitlin equations we have reported on a new technique for studying 2-D turbulence via canonical splitting of vorticity. In numerical simulations, this splitting dynamically develops into a separation of scales. These numerical results are supported by some theoretical evidence. To develop a full mathematical understanding of these

phenomena, even completely within the setting of Zeitlin's model, is an interesting open problem. We have further presented mathematical foundations for a weak L^∞ theory in the continuous setting, independent of Zeitlin's model.

As the numerical simulations so strikingly capture the scale separation process, and as the inverse relations of the corresponding energy–enstrophy splitting reflect the stationary theory of Kraichnan, further numerical and theoretical studies of the canonical vorticity splitting shall likely unveil more details on the mechanism behind vortex condensation. Furthermore, the splitting into large scales ω_s and small scales ω_r suggests using these variables as a basis for stochastic model reduction (cf. Jain, Timofeyev & Vanden-Eijnden 2015) of the 2-D Euler equations, with ω_r modelled as multiplicative noise.

Supplementary material and movies. Supplementary material and movies are available at https://doi.org/10.1017/jfm.2022.457.

Acknowledgements. The computations were enabled by resources provided by the Swedish National Infrastructure for Computing (SNIC) at C3SE partially funded by the Swedish Research Council through grant agreement no. 2018-05973.

Funding. This work was supported by the Swedish Research Council (K.M., grant number 2017-05040); the Knut and Alice Wallenberg Foundation (K.M., grant number WAF2019.0201), (M.V., grant number KAW2020.0287); and the research grant Junior Visiting Fellowship by the Scuola Normale Superiore of Pisa, Italy.

Declaration of interests. The authors report no conflict of interest.

Author ORCIDs.
Klas Modin https://orcid.org/0000-0001-6900-1122;
Milo Viviani https://orcid.org/0000-0002-2340-0483.

References

Abramov, R.V. & Majda, A.J. 2003 Statistically relevant conserved quantities for truncated quasigeostrophic flow. *Proc. Natl Acad. Sci. USA* **100** (7), 3841–3846.

Arnold, V.I. & Khesin, B.A. 1998 *Topological Methods in Hydrodynamics*. Springer.

Boffetta, G. & Ecke, R.E. 2012 Two-dimensional turbulence. *Annu. Rev. Fluid Mech.* **44** (1), 427–451.

Bouchet, F. & Venaille, A. 2012 Statistical mechanics of two-dimensional and geophysical flows. *Phys. Rep.* **515** (5), 227–295.

Caglioti, E., Lions, P.L., Marchioro, C. & Pulvirenti, M. 1992 A special class of stationary flows for two-dimensional Euler equations: a statistical mechanics description. *Commun. Math. Phys.* **143** (3), 501–525.

Caglioti, E., Lions, P.L., Marchioro, C. & Pulvirenti, M. 1995 A special class of stationary flows for two-dimensional Euler equations: a statistical mechanics description. Part II. *Commun. Math. Phys.* **174** (2), 229–260.

Chertkov, M., Connaughton, C., Kolokolov, I. & Lebedev, V. 2007 Dynamics of energy condensation in two-dimensional turbulence. *Phys. Rev. Lett.* **99**, 084501.

Couder, Y 1984 Two-dimensional grid turbulence in a thin liquid film. *J. Phys. (Paris)* **45** (8), 353–360.

Cullen, M. 2006 *A Mathematical Theory of Large-Scale Atmosphere/Ocean Flow*. Imperial College Press.

Dolzhansky, F.V. 2013 *Fundamentals of Geophysical Hydrodynamics*, vol. 103. Springer.

Dritschel, D.G., Qi, W. & Marston, J.B. 2015 On the late-time behaviour of a bounded, inviscid two-dimensional flow. *J. Fluid Mech.* **783**, 1–22.

Euler, L. 1757 Principes généraux de l'état d'équilibre d'un fluide. *Académie Royale des Sciences et des Belles-Lettres de Berlin, Mémoires* **11**, 217–273.

Eyink, G.L. & Sreenivasan, K.R. 2006 Onsager and the theory of hydrodynamic turbulence. *Rev. Mod. Phys.* **78** (1), 87–135.

Fairlie, D.B. & Zachos, C.K. 1989 Infinite-dimensional algebras, sine brackets, and SU(∞). *Phys. Lett.* B **224** (1–2), 101–107.

Farge, M., Schneider, K. & Kevlahan, N. 1999 Non-Gaussianity and coherent vortex simulation for two-dimensional turbulence using an adaptive orthogonal wavelet basis. *Phys. Fluids* **11** (8), 2187–2201.

GAUTHIER, G., REEVES, M.T., YU, X., BRADLEY, A.S., BAKER, M.A., BELL, T.A., RUBINSZTEIN-DUNLOP, H., DAVIS, M.J. & NEELY, T.W. 2019 Giant vortex clusters in a two-dimensional quantum fluid. *Science* **364** (6447), 1264–1267.

HERBERT, C. 2013 Additional invariants and statistical equilibria for the 2D Euler equations on a spherical domain. *J. Stat. Phys.* **152** (6), 1084–1114.

HOPPE, J. 1982 Quantum theory of a massless relativistic surface and a two-dimensional bound state problem. PhD thesis, MIT, Cambridge.

HOPPE, J. & YAU, S.-T. 1998 Some properties of matrix harmonics on S2. *Commun. Math. Phys.* **195**, 66–77.

JAIN, A., TIMOFEYEV, I. & VANDEN-EIJNDEN, E. 2015 Stochastic mode-reduction in models with conservative fast sub-systems. *Commun. Math. Sci.* **2** (13), 297–314.

JOHNSTONE, S.P., GROSZEK, A.J., STARKEY, P.T., BILLINGTON, C.J., SIMULA, T.P. & HELMERSON, K. 2019 Evolution of large-scale flow from turbulence in a two-dimensional superfluid. *Science* **364** (6447), 1267–1271.

KIESSLING, M.K.-H. 1993 Statistical mechanics of classical particles with logarithmic interactions. *Commun. Pure Appl. Maths* **46** (1), 27–56.

KIRILLOV, A.A. 2004 *Lectures on the Orbit Method*, vol. 64. American Mathematical Soc.

KOLMOGOROV, A.N. 1941 The local structure of turbulence in incompressible viscous fluid for very large Reynolds numbers. *Doklady Akademii Nauk SSSR* **30**, 299–303.

KRAICHNAN, R.H. 1967 Inertial ranges in two-dimensional turbulence. *Phys. Fluids* **10** (7), 1417–1423.

KRAICHNAN, R.H. 1975 Statistical dynamics of two-dimensional flow. *J. Fluid Mech.* **67** (1), 155–175.

KUKSIN, S. & SHIRIKYAN, A. 2012 *Mathematics of Two-Dimensional Turbulence*. Cambridge University Press.

KUKSIN, S. & SHIRIKYAN, A. 2017 Rigorous results in space-periodic two-dimensional turbulence. *Phys. Fluids* **29** (12), 125106.

LYNDEN-BELL, D. 1967 Statistical mechanics of violent relaxation in stellar systems. *Mon. Not. R. Astron. Soc.* **136**(1), 101–121.

MAJDA, A. & WANG, X. 2006 *Nonlinear Dynamics and Statistical Theories for Basic Geophysical Flows*. Cambridge University Press.

MAJDA, A.J. & BERTOZZI, A.L. 2002 *Vorticity and Incompressible Flow*. Cambridge University Press.

MARCHIORO, C. & PULVIRENTI, M. 2012 *Mathematical Theory of Incompressible Nonviscous Fluids*, vol. 96. Springer Science & Business Media.

MCLACHLAN, R. 1993 Explicit Lie–Poisson integration and the Euler equations. *Phys. Rev. Lett.* **71** (19), 3043–3046.

MILLER, J. 1990 Statistical mechanics of Euler equations in two dimensions. *Phys. Rev. Lett.* **65**, 2137–2140.

MODIN, K. & VIVIANI, M. 2020*a* A Casimir preserving scheme for long-time simulation of spherical ideal hydrodynamics. *J. Fluid Mech.* **884**, A22.

MODIN, K. & VIVIANI, M. 2020*b* Lie–Poisson numerical schemes for isospectral flows. *Found. Comput. Maths* **20**, 889–921.

MODIN, K. & VIVIANI, M. 2021 Integrability of point-vortex dynamics via symplectic reduction: a survey. *Arnold Math. J.* **7** (3), 357–385.

NASTROM, G.D., GAGE, K.S. & JASPERSON, W.H. 1984 Kinetic energy spectrum of large-and mesoscale atmospheric processes. *Nature* **310** (5972), 36–38.

ONSAGER, L. 1949 Statistical hydrodynamics. *Il Nuovo Cimento* **6** (2), 279–287.

PEDLOSKY, J. 2013 *Geophysical Fluid Dynamics*. Springer.

ROBERT, R. & SOMMERIA, J. 1991 Statistical equilibrium states for two-dimensional flows. *J. Fluid Mech.* **229**, 291–310.

SHNIRELMAN, A. 1993 Lattice theory and flows of ideal incompressible fluid. *Russ. J. Math. Phys.* **1** (1), 105–113.

SHNIRELMAN, A. 2013 On the long-time behavior of fluid flows. *Procedia IUTAM* **7**, 151–160.

SOMMERIA, J. 1988 Electrically driven vortices in a strong magnetic field. *J. Fluid Mech.* **189**, 553–569.

XIAO, Z., WAN, M., CHEN, S. & EYINK, G.L. 2009 Physical mechanism of the inverse energy cascade of two-dimensional turbulence: a numerical investigation. *J. Fluid Mech.* **619**, 1–44.

YUDOVICH, V.I. 1963 Non-stationary flows of an ideal incompressible fluid. *Zh. Vychisl. Mat. Mat. Fiz.* **3** (6), 1032–1066.

ZEITLIN, V. 1991 Finite-mode analogues of 2D ideal hydrodynamics: coadjoint orbits and local canonical structure. *Physica* D **49** (3), 353–362.

ZEITLIN, V. 2004 Self-consistent-mode approximation for the hydrodynamics of an incompressible fluid on non rotating and rotating spheres. *Phys. Rev. Lett.* **93** (26), 353–362.

ZEITLIN, V. 2018 *Geophysical Fluid Dynamics: Understanding (Almost) Everything with Rotating Shallow Water Models*. Oxford University Press.